Check for updates

Fluoride-bridged dinuclear dysprosium complex showing single-molecule magnetic behavior: supramolecular approach to isolate magnetic molecules†

Dong-Fang Wu,[a] Kiyonori Takahashi, [ID] *[ab] Masaru Fujibayashi, [ID][c] Naoto Tsuchiya,[c] Goulven Cosquer, [ID][c] Rui-Kang Huang, [ID][ab] Chen Xue, [ID][ab] Sadafumi Nishihara [ID][cd] and Takayoshi Nakamura*[ab]

Using Na-encapsulated benzo[18]crown-6 (Na)(B18C6) as a counter cation, we successfully magnetically isolated a fluoride-bridging Dy dinuclear complex {[(PW$_{11}$O$_{39}$)Dy(H$_2$O)$_2$]$_2$F} (Dy$_2$POM) with lacunary Keggin ligands. (Na)(B18C6) formed two types of tetramers through C−H···O, π···π and C−H···π interactions, and each tetramer aligned in one dimension along the *c*-axis to form two types of channels. One channel was partially penetrated by a supramolecular cation from the ±*a*-axis direction, dividing the channel in the form of a "bamboo node". Dy$_2$POM was spatially divided by this "bamboo node," which magnetically isolated one portion from the other. The temperature dependence of the magnetic susceptibility indicated a weak ferromagnetic interaction between the Dy ions bridged by fluoride. Dy$_2$POM exhibited the magnetic relaxation characteristics of a single-molecule magnet, including the dependence of AC magnetic susceptibility on temperature and frequency. Magnetic relaxation can be described by the combination of thermally active Orbach and temperature-independent quantum tunneling processes. The application of a static magnetic field effectively suppressed the relaxation due to quantum tunneling.

Introduction

Single-molecule magnets (SMMs) can be applied to ultra-high-density data storage,[1] quantum computing,[2] and spintronics[3] because of their nontrivial memory effect and quantum phenomena.[4–10] SMMs are molecules with energy barrier to spin reversal which induce magnetization without external magnetic field. This magnetization relaxes slowly in time at low temperature, resulting in a frequency dependence of the dynamic susceptibility. They are "molecule-sized permanent magnets" that exhibit magnetic hysteresis, although they have no magnetic long-range order. In order to observe this behaviour,

a well isolated Ising ground state must be favored.[11] In other word, the ground state should consist of pure m_J state with the greatest value and a large energy barrier. The pure m_J state will prevent the quantum tunneling of the magnetization whereas the energy barrier will prevent the thermal relaxation.[12] In the case of lanthanides based SMM, the electronic configuration can be controlled by an adjustment of the coordination environment around the ions.[13] A large magnetic anisotropy appears as a result of the interaction between the orbital angular momentum component and ligand field potential. Therefore, the use of lanthanides enables the creation of SMMs with single ions (single-ion magnets (SIMs)).[12,14–19]

Because the magnetic properties of SMMs originate from a single molecule, the molecules of SMMs must be magnetically separated within the crystal.[20–23] Several approaches have been reported to achieve magnetic shielding between magnetic molecules, utilizing bulky lacunary polyoxometalates (POMs) as ligands.[24–28] For example, E. Coronado *et al.* reported that [LnW$_{10}$O$_{36}$]$^{9-}$ (Ln = Tb, Dy, Ho, and Er), in which lacunary POMs sandwich lanthanide ions, exhibit magnetic relaxation characteristic of SMMs.[29] Larger lacunary POMs can be used to construct lanthanide multinuclear complexes.[26] In particular, the diamagnetic ligands Keggin and Wells-Dawson type lacunary heterotungstates can sandwich and magnetically isolate

[a] Graduate School of Environmental Science, Hokkaido University, N10W5, Kita-Ward, Sapporo, Hokkaido, 060-0810, Japan. E-mail: ktakahashi@es.hokudai.ac.jp; tnaka@es.hokudai.ac.jp

[b] Research Institute for Electronic Science (RIES), Hokkaido University, N20W10, Kita-Ward, Sapporo, Hokkaido 001-0020, Japan

[c] Department of Chemistry, Graduate School of Advanced Science and Engineering, Hiroshima University, Higashi-hiroshima, Hiroshima, 739-8527, Japan

[d] JST, PRESTO, Honcho 4-1-8, Kawaguchi, Saitama, 332-0012, Japan

multinuclear units, and a variety of lanthanoid multinuclear complexes have been synthesized.[25,26,28] For example, $(TBA)_{8.5}$-$H_{1.5}[(PW_{11}O_{39})_2Dy_2X_2(H_2O)_2]\cdot6H_2O$ (X = OH; F; OAc), in which the Dy dinuclear unit bridged by two F^-, OH^- or OAc^-, $Dy_2X_2(H_2O)_2$, is sandwiched by lacunary Keggin, is reported.[30] Bridging ligands between lanthanides play an important role in SMM behavior. In these crystals, the fluoride- and hydroxyde-bridged complexes exhibit SMM behavior with $U_{eff} = 98$ and $74\ cm^{-1}$, respectively, while the acetate-bridged complex does not exhibit SMM behavior.

It is also possible to use counter cations to spatially isolate the complex to ensure SMM behavior. We previously showed that supramolecular structures comprising crown ethers and inorganic or organic ammonium cations exhibit large amplitude motions such as molecular rotation in crystals.[31–37] The cation is isolated from the counter anion to ensure space for molecular motion in the crystal. For example, in the crystal of (4,4′-bipyridinium)(dibenzo[24]crown-8)[Ni(dmit)$_2$]$^-$, where dmit^{2-} = 1,3-dithio-2-thione-4,5-dithiolate, mono-protonated 4,4′-bipyridinium is connected via hydrogen bonds to form a pseudo polyrotaxane structure by penetrating dibenzo[24]crown-8.[38] One of the pyridine rings of 4,4′-bipyridinium exhibits rotational motion at about 293 K as a result of its isolation from the other molecules. Supramolecular cationic structures are also useful for isolating counter anions. In the case of $Cs_2([18]crown-6)_3[Ni(dmit)_2]_2^-$, [18]crown-6 rotates in the $Cs_2([18]crown-6)_3$ triple-decker structure.[37] The counter anion, $[Ni(dmit)_2]^-$, forms a dimer, which is completely isolated and surrounded by supramolecular cations.

In this study, we focused on a dinuclear Dy complex with a lacunary Keggin ligand.[39–41] To ensure the separation of the complex, (Na)(B18C6) (B18C6 = benzo[18]crown-6) supramolecular cations were introduced into the crystal. Within the crystal, (Na)(B18C6) formed two types of tetramers via C–H···O, π···π and C–H···π interactions, each of which was arranged in one dimension to form a bamboo-like channel structure. The fluoride-bridged Dy dinuclear complex coordinated with two lacunary Keggin ligands and four H_2O molecules. $\{[(PW_{11}O_{39})Dy(H_2O)_2]_2F\}$ (Dy$_2$POM) was divided by a "bamboo node" and completely isolated from the neighboring complexes. The crystals exhibited the magnetic relaxation characteristics of an SMM at low temperatures.

Results and discussion

Crystal structure

The crystal system and space group of $[(Na)(B18C6)(H_2O)_{0.5}]_2[(Na)(B18C6)(H_2O)_{1.5}]_2[(Na)(B18C6)(H_2O)]_2[(Na)(B18C6)(H_2O)_{1.75}]_2[((PW_{11}O_{39})Dy(H_2O)_2)_2F][(Na)(B18C6)]_2(F)\cdot12H_2O$ (1) are triclinic, $P\bar{1}$. Half of the Dy$_2$POM structure, four (Na)(B18C6) units coordinated by water molecules, $[(Na)(B18C6)(H_2O)_{1.75}]$, $[(Na)(B18C6)(H_2O)_{1.5}]$, $[(Na)_2(B18C6)_2(H_2O)]$ and $[(Na)_2(B18C6)_2(H_2O)_{0.5}]$, denoted as A–D, respectively, are crystallographically independent.

One water molecule with an occupancies of 0.5 in A, two water molecules with occupancies of 0.5 and 1 in B, one water molecule with an occupancy of 1 in C, and two water molecules

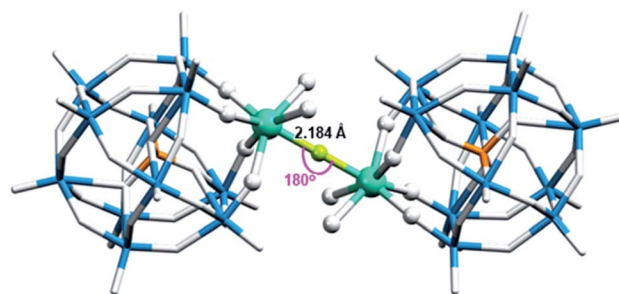Fig. 1 Structure of $\{[(PW_{11}O_{39})Dy(H_2O)_2]_2F\}$ in the crystal, with Dy-bridged fluoride at the symmetric center; Dy, O, W, F, and P are shown in green, white, blue, yellowish-green and orange, respectively. Dy, F, and O atoms coordinated to Dy are depicted as balls, and the others are shown as stick models. The minor disordered sites of O and W atoms are omitted for clarity.

with occupancies of 0.75 and 1.0 in D, respectively, were coordinated to Na$^+$ (Fig. S1†). In addition, six water molecules were isolated within the crystal as crystallographically independent guest molecules. Electron densities that could not be assigned to individual atoms were subtracted using the SQUEEZE function of the PLATON program.[42] The composition of the crystals was also determined from X-ray photoelectron spectroscopy (XPS). XPS measurements confirmed the presence of C, H, O, Dy, W, Na, and F atoms, but no B or N atoms were observed (Fig. S5†). The composition ratio of Na, P, and F was estimated to be 5 : 1 : 1 from SEM-EDX measurements (Fig. S6 and Table S2†), corresponding to the estimation about the number of (Na)(B18C6) and fluoride ion. Based on the elemental analyses and charge balance of the crystal, the two (Na)(B18C6) units and one fluoride ion should exist in the crystal in addition to the assigned molecules. The thermogravimetric analysis suggests that total number of the H_2O is approximately 28 (see Fig. S7†). The number of water molecules in the crystal 1 assigned by X-ray analysis is 25.5 per formula. There are about three H_2O molecules in the crystal that were not assigned by structural analysis. The electron density not assigned to individual atoms (224 e$^-$/mol) would consist of one (Na)(B18C6) unit (178 e$^-$/mol), one fluoride ion (10 e$^-$/mol), and about three H_2O molecules (10 e$^-$/mol each). Since crystal 1 would not form without (m-fluoroanilinium$^+$)(BF$_4^-$), the source of the F atom, we conclude that the fluoride-bridged Dy dinuclear complex is present in the crystal.[43]

Fig. 1 shows the structure of Dy$_2$POM. Lacunary POM ligand is disordered over two sites with the occupancy ratio of 0.556(8) : 0.444(8) (Fig. S2†). In Dy$_2$POM, four O atoms of the lacunary Keggin ligand, two O atoms of H_2O, and one F$^-$ ion are coordinated to the Dy atom. The two Dy atoms are bridged by fluoride located at the symmetric center to form a dinuclear complex.

In a complex of dinuclear Dy bridged by a single fluoride ion, Dy–F bond lengths of 2.137–2.315 Å and Dy–F–Dy angles of 169.8–180° have been reported.[44,45] The Dy–F bond lengths (2.184 Å) and Dy–F–Dy angles (180°) found in Dy$_2$POM are reasonable values. (Na)(B18C6) and H_2O molecules coordinated to Na form 1D supramolecular arrays. Fig. 2 shows the structure
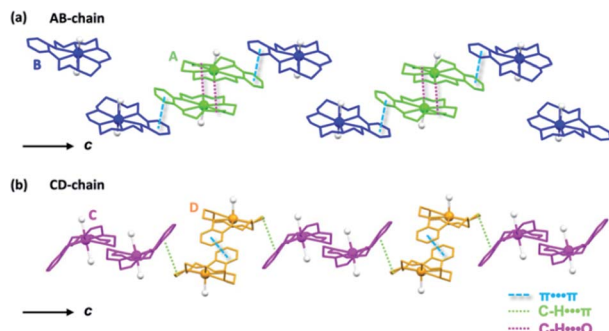
Fig. 2 One-dimensional (1D) array of supramolecular cations along the *c*-axis. The (Na)(B18C6) units of **A**, **B**, **C**, and **D** are shown in green, blue, magenta, and orange, respectively. The 1D chains of (a) **A** and **B** (**AB**-chain) and (b) **C** and **D** (**CD**-chain).

of the one-dimensional (1D) arrays of supramolecular cations. There are two types of (Na)(B18C6) supramolecular arrays: one comprising **A** and **B**, and the other comprising **C** and **D** (**AB**- and **CD**-chains, respectively). Each is arranged in one dimension along the *c*-axis. In the **AB**-chain, two **A** units formed a dimer by the C–H···O interaction, which formed a **B-A–A-B**-type tetramer with neighboring **B** *via* π···π interactions between the

phenylene groups. In the **CD**-chain, the two **D** units formed a dimer *via* π···π interactions. The –CH$_2$–CH$_2$- group of the **D** unit and the π plane of the phenylene ring of the **C** unit were in contact below the van der Waals radius, indicating that C–H···π interaction occurred between the **C** and **D** units. Consequently, a **C-D–D-C** tetramer was formed in the **CD**-chain. There was no strong interaction between the adjacent tetramers in either chain. Two types of channels parallel to the *c*-axis were formed (denoted as **Ch$_1$** and **Ch$_2$**, as shown in Fig. 3a). Channel **Ch$_1$** had minimum and maximum diameters of 6.2 and 10.5 Å, respectively, and was filled with two (Na)(B18C6) units and 12H$_2$O molecules, according to molecular formula (Fig. S3†). In contrast, **Ch$_2$** was partially penetrated by supramolecular cation **B** from the ±*a*-axes (Fig. 3b). As shown in Fig. 3b, the two supramolecular cations, **B**, penetrating **Ch$_2$** are the closest together at the H atom, with an H–H interatomic distance of 3.616 Å. **Ch$_2$** had a space with a minimum width of only 1.2 Å. No atoms could be assigned to the space between the two supramolecular cations of **C**. The **Ch$_2$** channel was divided into compartments separated by "bamboo nodes" as a result of the penetration of supramolecular cation **C**. Dy$_2$POM and two H$_2$O were embedded in each of the compartments separated by the bamboo nodes (Fig. 3d). The distance between the adjacent
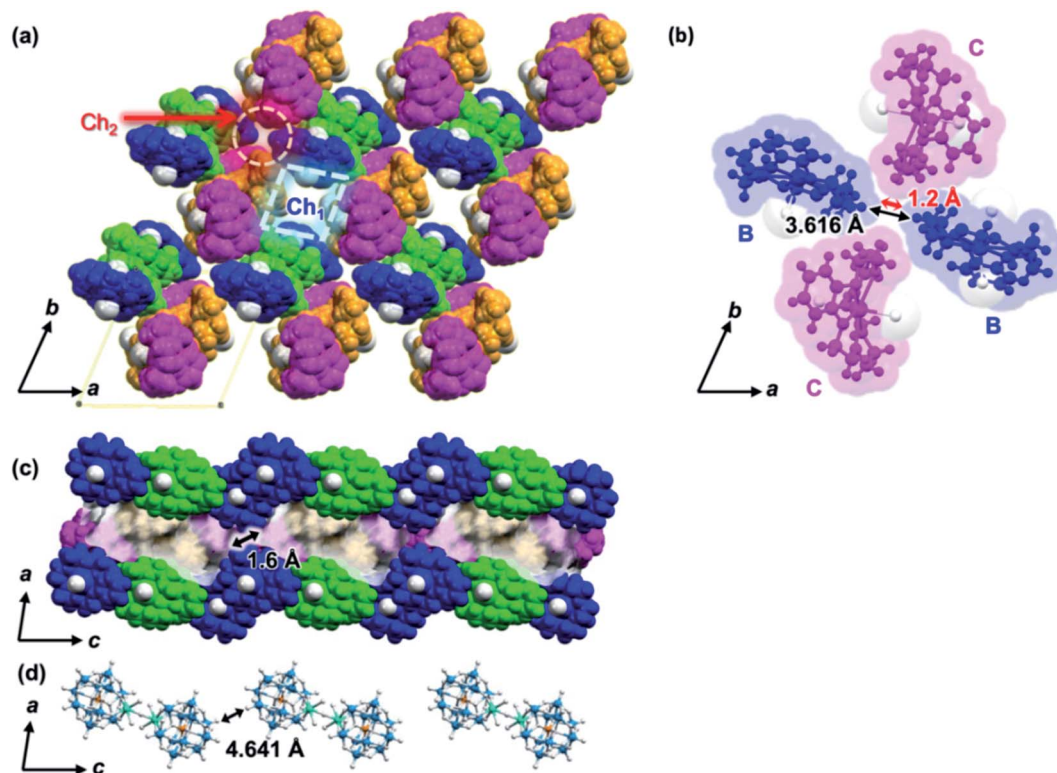

Fig. 3 Crystal structure of **1**. The colors of supramolecular cations **A**, **B**, **C**, and **D** are the same as in Fig. 2. Supramolecular cations are shown in the space filling model. H$_2$O molecules other than H$_2$O coordinated to Na and Dy are omitted. (a) *c*-Axis projection, showing the two types of 1D channels, **Ch$_1$** and **Ch$_2$**, formed along the *c*-axis direction are indicated by dotted line squares and circles, respectively. (b) Supramolecular cation **B** penetrating **Ch$_2$**, acting similar to a "bamboo node". Black and red arrows indicate the center-to-center (3.616 Å) and end-to-end distances (1.2 Å) of the nearest hydrogen atoms. (c) *b*-Axis projection showing compartments separated by bamboo nodes. (d) Alignment of Dy$_2$POM along the *c*-axis divided by bamboo nodes. The distance between adjacent Dy$_2$POM units is 4.641 Å, as measured between the centers of the nearest O atoms.

Dy$_2$POM units in the channel was 4.641 Å, as measured between the centers of the nearest O atoms (Fig. 3d). Considering the van der Waals radius of the O atom (1.52 Å), there was a space of 1.60 Å between the Dy$_2$POM ends along the *c*-axis (Fig. 3c). In addition, Dy$_2$POM was separated by (Na)(B18C6) in the *a*- and *b*-axes directions. The central F distances between adjacent Dy$_2$POM units were 17.566 and 17.872 Å along the *a*- and *b*-axes, respectively (Fig. S4†), while intramolecular Dy distance was 4.368 Å. The Dy$_2$POM units were spatially and therefore magnetically isolated from each other in the compartments between the bamboo nodes.

Magnetic properties

The temperature dependence of the molar magnetic susceptibility (χ_m) of crystal **1** is shown in Fig. S9.† The crystal exhibited ferromagnetic interactions, with $\chi_m T$ values considerably increasing with decreasing temperature below 30 K. These results indicated the existence of ferromagnetic interactions between Dy cations bridged by fluoride.[30,45,46] To investigate the magnetic dynamics of individual Dy$_2$POM units, the temperature and frequency dependences of the AC susceptibilities were measured. Fig. 4 shows the temperature and frequency dependences of the real (χ') and imaginary (χ'') parts of the magnetic susceptibilities under zero and 400 Oe direct magnetic fields. Even under the zero field, a remarkable frequency dependence

was observed, indicating that the Dy$_2$POM unit exhibited the slow relaxation of magnetization typical of SMMs. χ' gradually decreased with increasing frequency from 1 Hz at all temperatures. χ'' showed a maximum, and the peak shifted to higher frequencies at higher temperatures. Direct magnetic fields suppress the quantum tunneling of magnetization (QTM) process. The frequency dependence of AC magnetization at a direct magnetic field of 400 Oe is shown in Fig. 4b. Compared with the zero field, the χ''' peak shifted to a lower frequency. The QTM was efficiently suppressed in the presence of a direct magnetic field.[47]

Magnetic relaxation time (τ) was calculated using the single-relaxation Debye model (Fig. S10 and Tables S3 and S4†). The temperature dependence of $\ln(\tau)$ is shown in Fig. 5. The temperature dependence of τ was analyzed using the following equations:

$$\tau^{-1} = \tau_{QTM}^{-1} + \tau_0^{-1} \exp\left(-\frac{U_{eff}}{k_B T}\right), \tag{1}$$

$$\tau^{-1} = AH^4T + \tau_0^{-1} \exp\left(-\frac{U_{eff}}{k_B T}\right). \tag{2}$$

τ_{QTM} represents the temperature-independent QTM. The first term of eqn (2) represents the direct relaxation process,
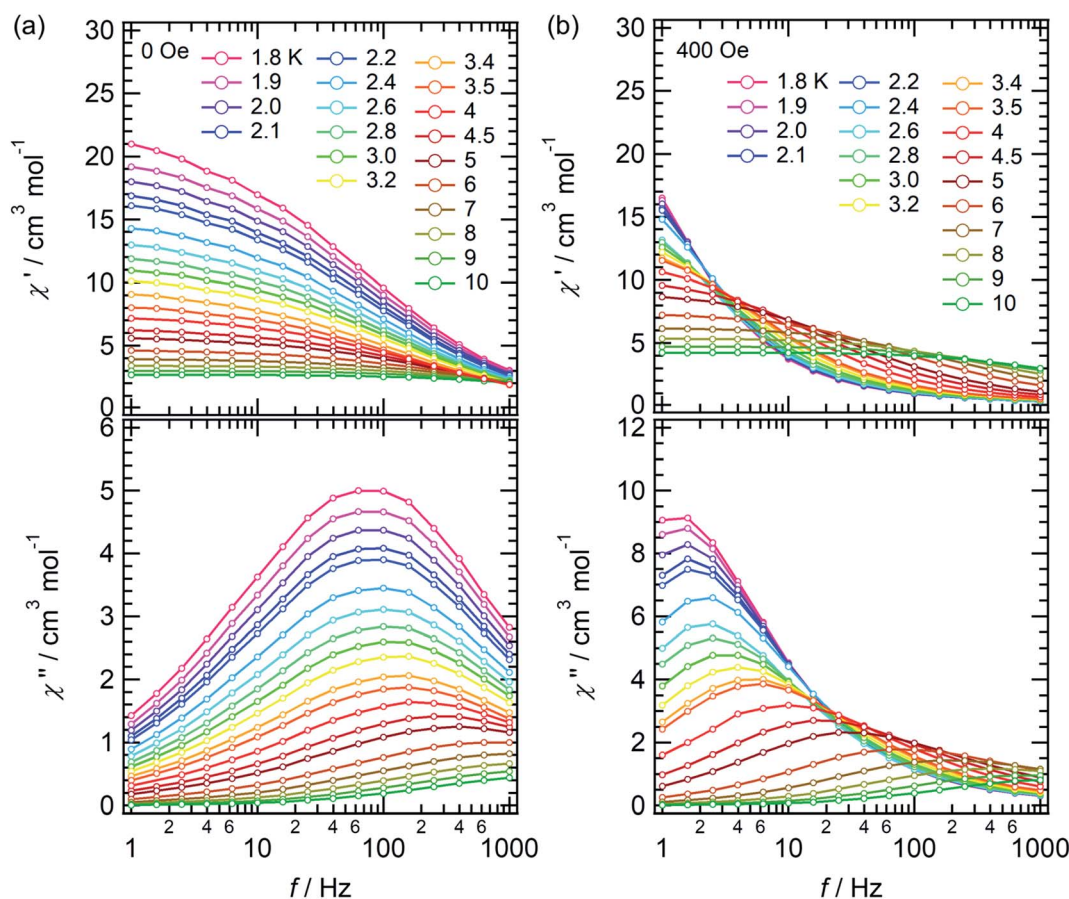

Fig. 4 Temperature and frequency dependence of in-phase (χ') and out-of-phase (χ'') products under (a) zero field and (b) 400 Oe direct magnetic field for the polycrystalline sample of **1**. The lines are a visual guide.
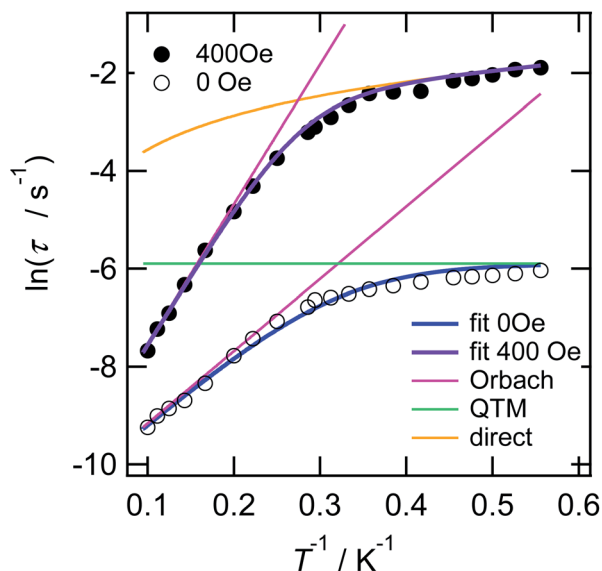
Fig. 5 Magnetic relaxation rate for crystal **1** by AC magnetometry under 0 and 400 Oe direct magnetic fields (note: log–log scale). Black-open and -closed circles correspond to the τ under 0 and 400 Oe direct magnetic fields, respectively. Blue and purple lines were fit with eqn (1) using U_{eff} = 14.8 K, τ_0 = 2.38 × 10^{-5} s, and τ_{QTM} = 2.74 × 10^{-3} s, and with eqn (2) using U_{eff} = 28.6 K, τ_0 = 3.04 × 10^{-5} s, and A = 1.37 × 10^{-10} Oe^{-4} K^{-1} s^{-1}, respectively. Magenta-, green- and orange-colored lines are the Orbach, QTM, and direct components, respectively.

where A is the fitting parameter, and H is the magnetic field. The second term represents the Orbach process of thermally activated relaxation. U_{eff} is the effective energy barrier for magnetization reversal, and k_B is Boltzmann's constant.[48] Without a direct magnetic field, a full model including various combination of QTM, Raman and Orbach relaxation process have been investigated to fit the experimental data, and the best result was obtained for the QTM + Orbach model (eqn (1)) with U_{eff}/k_B = 14.8 K, τ_0 = 2.38 × 10^{-5} s, and τ_{QTM} = 2.74 × 10^{-3} s. The obtained τ_0 and U_{eff}/k_B values were comparable to those of other reported Dy dinuclear SMMs.[49,50] The temperature dependence of τ was reproduced using eqn (2) with U_{eff}/k_B = 28.6 K, τ_0 = 3.04 × 10^{-5} s, and A = 1.37 × 10^{-10} Oe^{-4} K^{-1} s^{-1}. Because the temperature dependence of τ could be fitted with a direct term, QTM was effectively suppressed under a direct magnetic field of 400 Oe.

Experimental

Synthesis

General. All chemicals were of reagent grade and used as received. sodium tungstate(VI) dihydrate was procured from Wako Pure Chemical Industries (Osaka, Japan). DyCl$_3$·6H$_2$O was procured from the Merck Company. B18C6 and tetrafluoroboric acid were procured from Fujifilm Wako Chemicals (Osaka, Japan). m-Fluoroaniline was procured from TCI Fine Chemicals. The precursor lacunary Keggin, Na$_8$H[PW$_9$O$_{34}$], and sodium decatungstate (Na$_4$W$_{10}$O$_{32}$) were obtained according to the procedures reported in literature.[51] (m-

fluoroanilinium$^+$)(BF$_4$$^-$) was synthesized according to the procedures reported in literature.[31] The infrared spectrum of crystal **1** was measured using a Nicolet iS10 FTIR spectrum instrument equipped with an attenuated total reflection unit.

[(Na)(B18C6)(H$_2$O)$_{0.5}$]$_2$[(Na)(B18C6)(H$_2$O)$_{1.5}$]$_2$[(Na)(B18C6) (H$_2$O)]$_2$[(Na)(B18C6)(H$_2$O)$_{1.75}$]$_2$[((PW$_{11}$O$_{39}$)Dy(H$_2$O)$_2$)$_2$F] [(Na)(B18C6)]$_2$(F)·12H$_2$O (1). Solid DyCl$_3$·6H$_2$O was dissolved in 10 mL of H$_2$O during stirring, and a solution of Na$_2$CO$_3$ (1.00 M) was then slowly added, resulting in a pH level of 6.1. After the solution temperature reached 80 °C, Na$_8$H[PW$_9$O$_{34}$] (1.0 g, 0.42 mmol) was added, and the mixture was stirred at 80 °C for 1 h. The solution was then cooled to room temperature and centrifuged to remove insoluble material. The aqueous solution containing B18C6 (400 mg, 1.28 mmol) and (m-fluoroanilinium)(BF$_4$) (120 mg, 0.6 mmol) was added to the clear solution and stirred for 4 h at room temperature. After filtration, the filtrate was maintained for 1 day, resulting in colorless block crystals. Yield: 46% (based on Dy). Anal. calcd for C$_{160}$H$_{296.5}$Dy$_2$Na$_{10}$O$_{166.25}$F$_2$P$_2$W$_{22}$ (%): C 21.02, H 2.73; found (%): C 21.01, H 3.06, where calculations were based on a composition assuming that the water molecules of the guest and the water coordinated to Na were desorbed during the experimental manipulation. Selected IR data (ATR, cm^{-1}): 3643(m), 3458(w), 3129(w), 2921(w), 2873(m), 2712(w), 2280(w), 2111(w), 1630(w), 1594(m), 1503(s), 1450(s), 1351(m), 1289(w), 1250(s), 1214(s), 1118(s), 1086(m), 1038(s), 943(s), 881(s), 806(s), 744(w), 690(w), 592(w).

Characterization. Surface compositions of the crystal **1** were analysed using a JEOL JPS-9200 X-ray photoelectron spectrometer (XPS). Energy-dispersive X-ray spectroscopy (EDX) under scanning electron microscope (SEM), which was obtained by Hitachi SU8230 (Hitach High-tech), was performed and analysed by a Bruker Quantax EDS and ESPRIT software. Thermogravimetric differential thermal analyses (TG-DTA) were performed on Rigaku Thermo Plus TG-DTA 8120 thermal analysis station employing an Al$_2$O$_3$ reference sample, at the temperature range from room temperature to 800 °C at a heating rate of 5 K min^{-1} under a flow of N$_2$ gas (flow rate 50 mL min^{-1}).

Crystal structure analysis. The single-crystal X-ray diffraction measurements of all compounds were performed using a RIGAKU MicroMax-007HF diffractometer equipped with Cu Kα (λ = 1.54184 Å) X-ray radiation source and a Pilatus 200 K detector. A single crystal was mounted on CryoLoop (Hampton Research) with Paratone® 8277 (Hampton Research). Data collection, cell refinement, and data reduction were performed using CrysalisPRO (Rigaku Oxford Diffraction, 2017). The structures were determined using direct methods with SHELXT[52] and refined using full-matrix least-squares techniques on F^2 with SHELX[53] compiled in the OLEX2 package.[54] Crystal anisotropic thermal parameters were assigned to all non-hydrogen atoms. The CCDC deposition number was 2174802.†

Magnetic measurement. Magnetic susceptibility was measured using Quantum Design MPMS3 at the Faculty of Science, Hokkaido University, under 1000 Oe in a temperature range of 300–2 K. AC magnetic susceptibility measurements

© 2022 The Author(s). Published by the Royal Society of Chemistry

were conducted on an MPMS-5S SQUID magnetometer by the Science Faculty of Hiroshima University. Measurements were performed using a sample holder (plastic wrap). AC measurements were conducted during heating from 1.8 to 10 K, and the frequencies of AC magnetic susceptibility are shown in Fig. 4. The field (400 Oe) that best suppressed the QTM process during AC magnetic susceptibility measurement was determined *via* frequency-dependent AC magnetic susceptibility measurement at 1.8 K under several direct magnetic fields from 0 to 3000 Oe in the frequency range of 1–1000 Hz, as shown in Fig. S11.†

Conclusions

Using (Na)(B18C6) as a counter cation, we succeeded in isolating a fluoride-bridged dinuclear Dy complex with lacunary Keggin ligands (Dy$_2$POM) in the crystal. (Na)(B18C6) was one-dimensionally arranged in the crystal, forming a bamboo-like channel structure. Dy$_2$POM units were embedded between "bamboo nodes" and completely isolated from neighboring complexes. Thus, it was possible to evaluate the magnetic properties of Dy$_2$POM as a single molecule. Weak ferromagnetic interactions between Dy cations bridged by fluoride were observed. Magnetic relaxation proceeded *via* the Orbach process, and the absolute values of the effective energy barrier and relaxation time indicated that the SMM properties were essentially attributable to single ions.

There are two possible reasons for the observed SMM behaviour: the effect of the diamagnetic lacunary POM ligands and the effect of spatial isolation by supramolecular cations. The supramolecular approach is effective in achieving isolated SMM structures in crystals for complexes where spatial isolation is essential for SMM behaviour.[22] In future, we plan to test its usefulness with other SMM candidate molecules.

Author contributions

D. W.; synthesis, characterization, formal analysis, magnetic susceptibility measurements, writing – original draft. K. T., T. N.; supervision, conception, data curation, funding acquisition. M. F., N. T.; AC magnetic susceptibility measurements. G. C., S. N., K. T.; validation of magnetic property. D. W., K. T., R. H., C. X.; single crystal X-ray structural analysis. All authors contributed to the writing of the manuscript.

Conflicts of interest

We have no conflicts of interest to declare.

Acknowledgements

Notes and references

1 A. Zabala-Lekuona, J. M. Seco and E. Colacio, *Coord. Chem. Rev.*, 2021, **441**, 213984.

2 M. N. Leuenberger and D. Loss, *Nature*, 2001, **410**, 789–793.

3 L. Bogani and W. Wernsdorfer, *Nat. Mater.*, 2008, **73**, 179–186.

4 S. Hill, S. Datta, J. Liu, R. Inglis, C. J. Milios, P. L. Feng, J. J. Henderson, E. Del Barco, E. K. Brechin and D. N. Hendrickson, *Dalton Trans.*, 2010, **39**, 4693–4707.

5 R. Grindell, V. Vieru, T. Pugh, L. F. Chibotaru and R. A. Layfield, *Dalton Trans.*, 2016, **45**, 16556–16560.

6 X.-D. Shao, X. Zhang, C. Shi, Y.-F. Yao and W. Zhang, *Adv. Sci.*, 2015, **2**, 1500029.

7 X. L. Li and J. Tang, *Dalton Trans.*, 2019, **48**, 15358–15370.

8 S. Lee and T. Ogawa, *Chem. Lett.*, 2017, **46**, 10–18.

9 P. Abbasi, K. Quinn, D. I. Alexandropoulos, M. Damjanović, W. Wernsdorfer, A. Escuer, J. Mayans, M. Pilkington and T. C. Stamatatos, *J. Am. Chem. Soc.*, 2017, **139**, 15644–15647.

10 D. N. Woodruff, R. E. P. Winpenny and R. A. Layfield, *Chem. Rev.*, 2013, **113**, 5110–5148.

11 J. M. Frost, K. L. M. Harriman and M. Murugesu, *Chem. Sci.*, 2016, **7**, 2470–2491.

12 S. T. Liddle and J. Van Slageren, *Chem. Soc. Rev.*, 2015, **44**, 6655–6669.

13 Y. Gil, A. Castro-Alvarez, P. Fuentealba, E. Spodine and D. Aravena, *Chem.–Eur. J.*, 2022, DOI: 10.1002/CHEM.202200336.

14 N. Ishikawa, M. Sugita, T. Ishikawa, S. Y. Koshihara and Y. Kaizu, *J. Am. Chem. Soc.*, 2003, **125**, 8694–8695.

15 F. Pointillart, O. Cador, B. Le Guennic and L. Ouahab, *Coord. Chem. Rev.*, 2017, **346**, 150–175.

16 K. Katoh, H. Isshiki, T. Komeda and M. Yamashita, *Coord. Chem. Rev.*, 2011, **255**, 2124–2148.

17 Z. Zhu, M. Guo, X. L. Li and J. Tang, *Coord. Chem. Rev.*, 2019, **378**, 350–364.

18 P. Zhang, Y. N. Guo and J. Tang, *Coord. Chem. Rev.*, 2013, **257**, 1728–1763.

19 A. Dey, P. Kalita and V. Chandrasekhar, *ACS Omega*, 2018, **3**, 9462–9475.

20 S. Kanegawa, S. Karasawa, M. Nakano and N. Koga, *Chem. Commun.*, 2004, 1750–1751.

21 S. Karasawa, G. Zhou, H. Morikawa and N. Koga, *J. Am. Chem. Soc.*, 2003, **125**, 13676–13677.

22 S. Kanegawa, S. Karasawa, M. Maeyama, M. Nakano and N. Koga, *J. Am. Chem. Soc.*, 2008, **130**, 3079–3094.

23 S. Kanegawa, S. Karasawa, M. Nakano and N. Koga, *Bull. Chem. Soc. Jpn.*, 2006, **79**, 1372–1382.

24 W. Cañón-Mancisidor, G. Paredes-Castillo, P. Hermosilla-Ibáñez, D. Venegas-Yazigi, O. Cador, B. Le Guennic and F. Pointillart, *Eur. J. Inorg. Chem.*, 2021, **2021**, 4596–4609.

25 P. Ma, F. Hu, Y. Huo, D. Zhang, C. Zhang, J. Niu and J. Wang, *Cryst. Growth Des.*, 2017, **17**, 1947–1956.

26 X. Ma, W. Yang, L. Chen and J. Zhao, *CrystEngComm*, 2015, **17**, 8175–8197.

27 W. Cañón-Mancisidor, M. Zapata-Lizama, P. Hermosilla-Ibáñez, C. Cruz, D. Venegas-Yazigi and G. Mínguez Espallargas, *Chem. Commun.*, 2019, **55**, 14992–14995.

28 M. Vonci, C. Boskovic, M. Vonci and C. Boskovic, *Aust. J. Chem.*, 2014, **67**, 1542–1552.

29 M. A. AlDamen, J. M. Clemente-Juan, E. Coronado, C. Martí-Gastaldo and A. Gaita-Ariño, *J. Am. Chem. Soc.*, 2008, **130**, 8874–8875.

30 Y. Huo, Y. C. Chen, S. G. Wu, J. L. Liu, J. H. Jia, W. Bin Chen, B. L. Wang, Y. Q. Zhang and M. L. Tong, *Inorg. Chem.*, 2019, **58**, 1301–1308.

31 S. Nishihara, T. Akutagawa, D. Sato, S. Takeda, S. I. Noro and T. Nakamura, *Chem.–Asian J.*, 2007, **2**, 1083–1090.

32 T. Akutagawa, D. Sato, Q. Ye, T. Endo, S. I. Noro, S. Takeda and T. Nakamura, *Dalton Trans.*, 2010, **39**, 8219–8227.

33 T. Akutagawa, D. Endo, F. Kudo, S. I. Noro, S. Takeda, L. Cronin and T. Nakamura, *Cryst. Growth Des.*, 2008, **8**, 812–816.

34 T. Akutagawa, H. Koshinaka, D. Sato, S. Takeda, S.-I. Noro, H. Takahashi, R. Kumai, Y. Tokura and T. Nakamura, *Nat. Mater.*, 2009, **8**, 342–347.

35 T. Nakamura, T. Akutagawa, K. Honda, A. E. Underhill, A. T. Coomber and R. H. Friend, *Nature*, 1998, **394**, 159–162.

36 D. Sato, T. Akutagawa, S. Takeda, S. Noro and T. Nakamura, *Inorg. Chem.*, 2007, **46**, 363–365.

37 T. Akutagawa, K. Shitagami, S. Nishihara, S. Takeda, T. Hasegawa, T. Nakamura, Y. Hosokoshi, K. Inoue, S. Ikeuchi, Y. Miyazaki and K. Saito, *J. Am. Chem. Soc.*, 2005, **127**, 4397–4402.

38 Y. Shirakawa, K. Takahashi, H. Sato, N. Hoshino, H. Anetai, S. Noro, T. Akutagawa and T. Nakamura, *Chem.–Eur. J.*, 2019, **25**, 6920–6927.

39 M. J. Giansiracusa, M. Vonci, W. Van Den Heuvel, R. W. Gable, B. Moubaraki, K. S. Murray, D. Yu, R. A. Mole, A. Soncini and C. Boskovic, *Inorg. Chem.*, 2016, **55**, 5201–5214.

40 D. L. Long, R. Tsunashima and L. Cronin, *Angew. Chem., Int. Ed.*, 2010, **49**, 1736–1758.

41 Z. M. Zhang, S. Yao, Y. G. Li, H. H. Wu, Y. H. Wang, M. Rouzières, R. Clérac, Z. M. Su and E. B. Wang, *Chem. Commun.*, 2013, **49**, 2515–2517.

42 A. L. Spek, *Acta Crystallogr., Sect. C: Struct. Chem.*, 2015, **71**, 9–18.

43 W. Cañón-Mancisidor, C. J. Gómez-García, G. M. Espallargas, A. Vega, E. Spodine, D. Venegas-Yazigi and E. Coronado, *Chem. Sci.*, 2013, **5**, 324–332.

44 J. Corredoira-Vázquez, C. González-Barreira, M. Fondo, A. M. García-Deibe, J. Sanmartín-Matalobos, S. Gómez-Coca, E. Ruiz and E. Colacio, *Inorg. Chem.*, 2022, **61**(26), 9946–9959.

45 G. Brunet, F. Habib, I. Korobkov and M. Murugesu, *Inorg. Chem.*, 2015, **54**, 6195–6202.

46 Q. Zhou, F. Yang, D. Liu, Y. Peng, G. Li, Z. Shi and S. Feng, *Inorg. Chem.*, 2012, **51**, 7529–7536.

47 P. Kalita, J. Goura, J. Manuel Herrera Martínez, E. Colacio and V. Chandrasekhar, *Eur. J. Inorg. Chem.*, 2019, **2019**, 212–220.

48 M. Gonidec, F. Luis, À. Vílchez, J. Esquena, D. B. Amabilino, J. Veciana, M. Gonidec, D. B. Amabilino, J. Veciana, F. Luis, À. Vílchez and J. Esquena, *Angew. Chem., Int. Ed.*, 2010, **49**, 1623–1626.

49 W. Y. Zhang, Y. M. Tian, H. F. Li, P. Chen, W. Bin Sun, Y. Q. Zhang and P. F. Yan, *Dalton Trans.*, 2016, **45**, 3863–3873.

50 Y. F. Wang, C. L. Xue, S. C. Luo, Z. L. Wu and W. M. Wang, *J. Mol. Struct.*, 2021, **1232**, 130070.

51 R. Khoshnavazi, F. Nicolò, H. Amiri Rudbari, E. Naseri and A. Aminipour, *J. Coord. Chem.*, 2013, **66**, 1374–1383.

52 G. M. Sheldrick, *Acta Crystallogr., Sect. A: Found. Adv.*, 2015, **71**, 3–8.

53 G. M. Sheldrick, *Acta Crystallogr., Sect. C: Struct. Chem.*, 2015, **71**, 3–8.

54 O. V Dolomanov, L. J. Bourhis, R. J. Gildea, J. A. K. Howard and H. Puschmann, *J. Appl. Crystallogr.*, 2009, **42**, 339–341.